

# Relativistic Band-Structure Calculations for $\text{CeTIn}_5$ ( $T = \text{Ir}$ and $\text{Co}$ ) and Analysis of the Energy Bands by Using Tight-Binding Method

Takahiro Maehira<sup>1</sup>, Takashi Hotta<sup>1</sup>, Kazuo Ueda<sup>2,1</sup>, and Akira Hasegawa<sup>3</sup>

<sup>1</sup>Advanced Science Research Center, Japan Atomic Energy Research Institute, Tokai, Ibaraki 319-1195

<sup>2</sup>Institute for Solid State Physics, University of Tokyo, Kashiwa, Chiba 277-8581

<sup>3</sup>Niigata University, Niigata, Niigata 950-2181

(Received April 14, 2024)

In order to investigate electronic properties of recently discovered heavy fermion superconductors  $\text{CeTIn}_5$  ( $T = \text{Ir}$  and  $\text{Co}$ ), we employ the relativistic linear augmented-plane-wave (RLAPW) method to clarify the energy band structures and Fermi surfaces of those materials. The obtained energy bands mainly due to the large hybridization between Ce 4f and In 5p states well reproduce the Fermi surfaces consistent with the de Haas-van Alphen experimental results. However, when we attempt to understand magnetism and superconductivity in  $\text{CeTIn}_5$  from the microscopic viewpoint, the energy bands obtained in the RLAPW method are too complicated to analyze the system by further including electron correlations. Thus, it is necessary to prepare a more simplified model, keeping correctly the essential characters of the energy bands obtained in the band-structure calculation. For the purpose, we construct a tight-binding model for  $\text{CeTIn}_5$  by including f-f and p-p hoppings as well as f-p hybridization, which are expressed by the Slater-Koster integrals, determined by the direct comparison with the band-calculation result. Similarity and difference between  $\text{CeIrIn}_5$  and  $\text{CeCoIn}_5$  are discussed based on the obtained tight-binding model, suggesting a significant importance of the effect of crystalline electric field to understand the difference in electronic properties among  $\text{CeTIn}_5$ .

KEYWORDS: Relativistic linear APW method,  $\text{CeIrIn}_5$ ,  $\text{CeCoIn}_5$ , Fermi surface, tight-binding model

## x1. Introduction

Since the establishment of the density functional theory,<sup>1)</sup> the band-structure calculation method has been developed as a powerful and practical tool to analyze electronic properties of various kinds of materials from the first-principle viewpoint. Especially, due to the recent rapid developments in computational technology, significant improvements have been achieved in the potential of the band-structure calculation.<sup>2)</sup> For instance, nowadays it is possible to treat the complicated system including one hundred atoms in the unit cell.

On the other hand, in order to include electron correlation effects beyond the Hartree-Fock approximation, much efforts have been made to improve the local-density approximation (LDA). Along this direction, there have been steady improvements in approximations, such as the generalized gradient approximation<sup>3)</sup> and LDA+U method.<sup>4)</sup> However, since this is essentially a trial to include the many-body effect with high accuracy, it is difficult to obtain rapid improvements along this direction, although it is a challenging and crucial problem in the research field of condensed matter theory. In addition, even if such an improved approximation has been established in many-body physics, there still remains another important step to incorporate it into the band-structure calculation. Although this difficulty is believed to be overcome in future, at least at present, it becomes a hard task to have significant developments inmediately.

However, numbers of target materials of the band-structure calculation has been rapidly increased. Typ-

ically, strongly correlated electron systems such as transition metal oxides and f-electron compounds have attracted much attentions in recent decades. In the research field of strongly correlated electron systems, novel magnetism and unconventional superconductivity have been the central topics both from experimental and theoretical sides. In order to understand those intriguing phenomena, it is essentially important to include correlation effects based on the concrete knowledge on electronic properties.

For the purpose, it is necessary to promote a couple of theoretical researches in parallel with different viewpoints. Namely, one research is to analyze precisely the energy-band structure and Fermi surfaces by using the appropriate band-structure calculation techniques, in order to obtain correct information about the electronic properties around the Fermi energy, which can be directly compared with the result of the angle resolved photoemission experiment. Another is to construct a simplified tight-binding model to reproduce well the energy-band structure around the Fermi energy, in order to include the effect of electron correlation in this simplified model. We believe that those two types of researches should be complementary to each other in order to make significant progress in our understandings on novel magnetism and unconventional superconductivity, although it is quite important to develop methods and techniques in each research.

As is well known, the above framework works quite well in 3d-electron materials. For instance, in high- $T_c$  cuprates, the result of the band-structure calcula-

tion based on the LDA can be reproduced well by using the tight-binding model. Further adding short-range Coulomb interactions to this tight-binding model, we can obtain the so-called Hubbard Hamiltonian, which has been widely accepted as a canonical model for 3d electron systems. Based on the Hubbard Hamiltonian, it has been successful to understand several anomalous properties of high- $T_c$  cuprates. Note that this success is not due to the speciality of 3d electron. Also in the 4d electron system such as  $\text{Sr}_2\text{RuO}_4$ , which is an exotic material exhibiting triplet superconductivity,<sup>5)</sup> three-band Hubbard Hamiltonian can reproduce well the Fermi surface structure and it becomes an appropriate microscopic model to investigate magnetism and superconductivity in ruthenates.<sup>6)</sup>

When we turn our attentions to superconductivity in f-electron systems, unfortunately, our understandings have been almost limited in the phenomenological level. One reason is that in f-electron compounds, the band-structure calculation method itself should be improved, since the relativistic effect cannot be simply neglected in those materials. In general, the Coulomb interaction between nucleus and electrons in proportion to the atomic number becomes very strong in ions including f electrons, indicating that the velocity of electron included in lanthanide and actinide ions easily becomes a fraction of light velocity. A simple way to take into account such a relativistic effect is to treat the spin-orbit interaction as a perturbation in the non-relativistic band-structure calculation method, leading to a handy method to grasp the feature of some f-electron compounds. However, this is not the first-principle method to take into account the relativistic effect, since the magnitude of spin-orbit interaction should be adjusted by hand. This point has been improved by the relativistic band-structure calculation technique, where the Dirac equations, not the non-relativistic Schrodinger equations, are directly solved to determine the one-electron state.<sup>7)</sup> After the improvements by Hasegawa and co-workers,<sup>8,9,10)</sup> it has been possible to obtain the reliable electronic band-structure and reproduce correctly the de Haas-van Alphen (dHvA) experimental results for f-electron systems.

Due to the developments in the relativistic band-structure calculation techniques, we seem to recover the situation quite similar to that of d-electron systems, namely, the tight-binding model can be constructed due to the comparison with the relativistic band-structure calculations for f-electron systems. However, we should note that due to the large spin-orbit coupling, the meaning of one-electron state becomes complicated in f-electron systems, in which the total angular momentum  $j$ , neither spin nor orbital degree of freedom, is the only good quantum number to specify the one-electron state at each site. Thus, it is still a non-trivial problem to construct the tight-binding model for f-electron systems, even if the relativistic band-structure calculation results are at hand. In this paper, we attempt to show that it is possible to construct the tight-binding model for f-electron systems by using the basis to diagonalize the z-component of total angular momentum  $j$ , so as to reproduce the result of the relativistic band-structure cal-

ulation. Then, it is suggested that such a model should be useful for the further microscopic discussion on magnetism and superconductivity in f-electron compounds.

As a typical example for our trial to construct the model, in this paper we focus on recently discovered Ce-based superconducting compounds  $\text{CeTIn}_5$  ( $T = \text{Rh, Ir, and Co}$ ),<sup>11,12,13)</sup> which are frequently referred to as "Ce-115" materials. A surprising point is that  $\text{CeCoIn}_5$  exhibits the superconducting transition temperature  $T_c = 2.3\text{K}$ , which is the highest among yet observed for heavy fermion materials at ambient pressure. On the other hand,  $\text{CeIrIn}_5$  shows  $T_c = 0.4\text{K}$  which is much less than that of  $\text{CeCoIn}_5$ . Note that  $\text{CeRhIn}_5$  is antiferromagnet with the Néel temperature  $T_N = 3.8\text{K}$  at ambient pressure, while under high-pressure it becomes superconducting with  $T_c = 2.1\text{K}$ . It is not well understood what is the key issue to characterize the difference in the ground state of these Ce-115 compounds. In order to clarify this point, it is necessary to establish a simplified model to include electron correlation effects from the microscopic viewpoint.

Among Ce-115 compounds, the dHvA effect has been successfully observed in  $\text{CeIrIn}_5$  and  $\text{CeCoIn}_5$ ,<sup>14,15)</sup> both of which have the huge electronic specific heat coefficient as large as several hundreds  $\text{mJ/K}^2 \text{mol}$ . The angular dependence of major experimental dHvA frequency branches is well explained by a quasi two-dimensional Fermi surface,<sup>14,15)</sup> which is a clear advantage when we construct a model Hamiltonian, since we can restrict ourselves in the two-dimensional case. This is another reason why we choose the Ce-115 compound as a typical example to attempt to construct a tight-binding model.

In this paper, first we employ the relativistic band-structure calculation method for  $\text{CeTIn}_5$  ( $T = \text{Ir and Co}$ ) to investigate the electronic properties in detail. It is found that there exists only a small difference between  $\text{CeIrIn}_5$  and  $\text{CeCoIn}_5$  in the energy bands around the Fermi level and the structure of Fermi surfaces. Namely, within the band-structure calculations, those two compounds cannot be distinguished, although  $T_c$ 's are quite different. Such a difference should originate from the issue with small energy-scale which cannot be included in the band-structure calculations. Then, in order to investigate such a small energy scale feature, we construct a tight-binding model including Ce 4f and In 5p electrons, and determine several parameters in the model by comparing with the band-structure calculation results. We reanalyze the electronic properties of  $\text{CeTIn}_5$  to clarify that the effect of crystalline electric field (CEF) is a key issue to distinguish  $\text{CeIrIn}_5$  and  $\text{CeCoIn}_5$ .

The organization of this paper is as follows. In Sec. 2, we show the relativistic band-structure calculation results both for  $\text{CeIrIn}_5$  and  $\text{CeCoIn}_5$ , to discuss the obtained energy band structure and the Fermi surfaces. In Sec. 3, we construct the tight-binding model for  $\text{CeTIn}_5$  by using the Slater-Koster integrals. Then, we make comparison between the relativistic band-structure calculation results and the dispersion obtained from our tight binding model. Finally in Sec. 4, we summarize this paper. Throughout this paper we use the energy units as  $k_B = \hbar = 1$ .

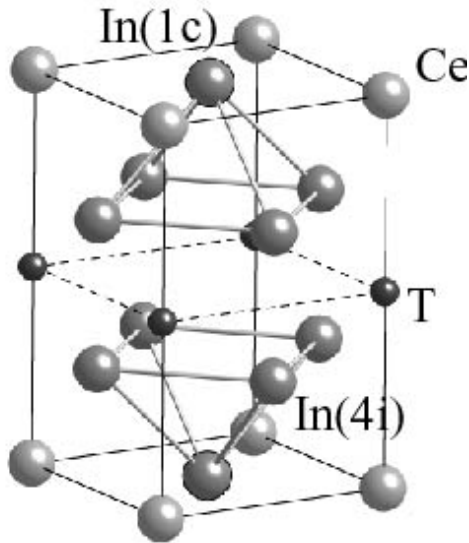


Fig. 1. Crystal structure of CeTIn<sub>5</sub>, called the HoCoGa<sub>5</sub>-type tetragonal structure.

Table I. Lattice constants and atomic positions of CeIrIn<sub>5</sub> and CeCoIn<sub>5</sub> determined experimentally.<sup>14)</sup> The labels for atoms are referred in Fig. 1.

	CeIrIn <sub>5</sub>	CeCoIn <sub>5</sub>
a	4.666 Å (= 8.818 a.u.)	4.612 Å (= 8.714 a.u.)
c	7.516 Å (= 14.205 a.u.)	7.549 Å (= 14.264 a.u.)
Ce	(0, 0, 0)	(0, 0, 0)
Ir	(0, 0, 1/2)	(0, 0, 1/2)
In(1c)	(1/2, 1/2, 1/2)	(1/2, 1/2, 1/2)
In(4i)	(0, 1/2, 0.30528)	(0, 1/2, 0.305)
	(1/2, 0, 0.30528)	(1/2, 0, 0.305)

## x2. Energy Band Calculations for CeTIn<sub>5</sub>

In order to calculate the electronic energy band structure of cerium compounds, in general, relativistic effects should be seriously taken into account.<sup>8)</sup> As is well known, in the hydrogen atom,  $v/c$  is just equal to the fine structure constant  $1/137$ , which is negligibly small, where  $v$  is the velocity of electron and  $c$  is the light velocity. However, in the atom with the atomic number  $Z$ ,  $v/c$  for the electron in the most inner orbital ( $K$ -shell) is given by  $Z=137$ , indicating that the velocity of the  $K$ -shell electron in the uranium atom with  $Z = 92$  becomes 67% of the light velocity. This is simply understood as follows: Due to the strong Coulomb attraction enhanced by  $Z$ , electrons near the heavy nucleus must move with a high speed in order to keep their stationary motion. Thus, the relativistic effect on the inner electrons becomes more significant in an atom with larger  $Z$ .

In order to take into account major relativistic effects such as the relativistic energy shifts, the relativistic screening effects, and the spin-orbit interaction in the energy band structure calculation, Loucks has derived a relativistic augmented plane wave (APW) method based on the Dirac one-electron wave equation.<sup>7)</sup> Al-

though his method was a natural extension of Slater's non-relativistic APW method to a relativistic theory, it included a couple of problems. For instance, the symmetrization of the basis functions was not taken into account and the method was not self-consistent. These points have been improved by Yamagami and Hasegawa.<sup>9)</sup> Note that Andersen has first suggested a linearized technique to include the relativistic effect in the APW method.<sup>16)</sup>

Among several methods, in this paper we employ a relativistic linear augmented-plane-wave (RLAPW) method. The exchange and correlation potential is considered within LDA, while the spatial shape of the one-electron potential is determined in the muffin-tin approximation. The self-consistent calculation is performed by using the lattice constants which are determined experimentally.

## 2.1 Basic properties of CeTIn<sub>5</sub>

Ce-115 materials are categorized into the HoCoGa<sub>5</sub>-type tetragonal structure as shown in Fig. 1, which is characterized by the space group  $P4mm$  (No. 123) and  $D_{4h}^{14}$ . Note that one molecule is contained per primitive cell. The lattice constants  $a$  and  $c$  as well as positions of all atoms in the unit cell are listed in Table I.

The  $4f$  electrons in CeTIn<sub>5</sub> ( $T = \text{Ir and Co}$ ) are assumed to be itinerant. The iteration process for solving the Dirac one-electron equation starts with the crystal charge density that is constructed by superposing the relativistic atomic charge densities for neutral atoms Ce ( $[Xe]4f^{14}5d^16s^2$ ), Co ( $[Ar]3d^74s^2$ ), Ir ( $[Xe]4f^{14}5d^76s^2$ ), and In ( $[Kr]4d^{10}5p^15s^2$ ), where  $[Xe]$ ,  $[Ar]$ , and  $[Kr]$  symbolically indicate the closed electronic configuration for xenon, argon, and krypton, respectively. In the calculation for the atoms, the same exchange and correlation potential are used as for the crystal. We assume that the Xe core state except the  $5p^6$  state for Ce, the Xe core state into the  $4f^{14}$  for Ir, the Ar core state for Co, and the Kr core state for In are unchanged during the iteration. Namely, the frozen-core approximation is adopted for these core states in the calculation for the crystal. In the relativistic atomic calculation, the spin-orbit splitting in the Ce  $4f$ , Ce  $5d$ , Co  $3d$ , Ir  $5d$ , and In  $5p$  state are found to be 25 mRyd., 15 mRyd., 14 mRyd., 90 mRyd., and 18 mRyd., respectively. Note here that mRyd. denotes milli-Rydberg and 1 Ryd. = 13.6 eV.

In each iteration step for the self-consistent calculation processes, a new crystal charge density is constructed using eighteen  $k$  points, which are uniformly distributed in the irreducible  $1/16$  part of the Brillouin zone. At each  $k$  in the Brillouin zone, 431 plane waves are adopted under the condition  $|\mathbf{k} + \mathbf{G}_j| < 2/a$  with  $\mathbf{G}$  the reciprocal lattice vector, and angular momentum up to  $l_{max} = 8$  are taken into account.

## 2.2 Results for CeIrIn<sub>5</sub>

First let us discuss the calculated results for CeIrIn<sub>5</sub>, as shown in Fig. 2, in which we depict the energy band structure along the symmetry axes in the Brillouin zone in the energy region from 0.5Ryd. to 1.0Ryd. Note here that the three Ce  $5p$  and twenty-five In  $4d$  bands in

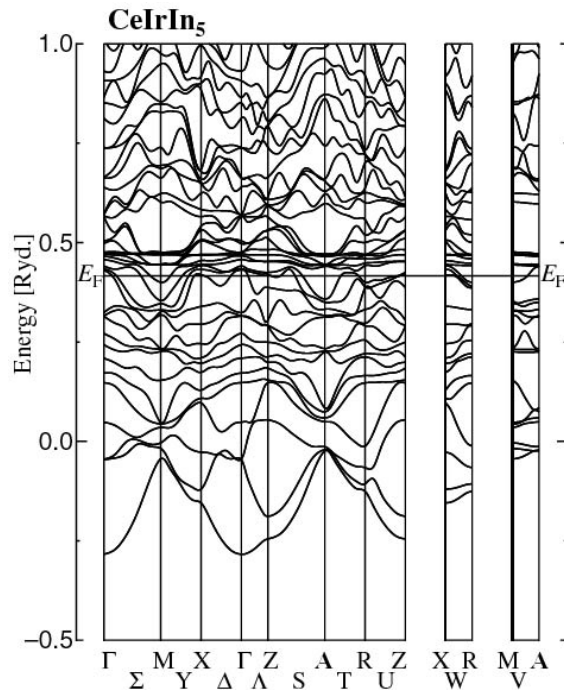


Fig. 2. Energy band structure for CeIrIn<sub>5</sub> calculated by using the self-consistent LAPW method.  $E_F$  indicate the position of the Fermi level.

Table II. The number of valence electrons in the Ce APW sphere, the Ir APW sphere, and the In APW sphere partitioned into angular momentum.

	s	p	d	f
Ce	0.28	6.16	2.05	1.25
Ir	0.54	0.38	7.33	0.02
In (1c)	1.02	0.66	9.84	0.01
In (4i)	3.74	2.69	39.31	0.09

the energy range between 1.0 Ryd. and 0.6 Ryd. are not shown in Fig. 2, since those bands are irrelevant to the present discussion. The Fermi level  $E_F$  is located at 0.416 Ryd. and in the vicinity of  $E_F$ , there occurs a hybridization between the Ce 4f and In 5p states. Above  $E_F$  near M point, the 4f bands split into two groups, corresponding to the total angular momentum  $j=5/2$  (lower bands) and  $7/2$  (upper bands). The magnitude of the splitting between those groups is estimated as 0.4 eV, which is almost equal to the spin-orbit splitting in the atomic 4f state.

The number of the valence electrons in the APW sphere is partitioned into the angular momentum and listed in Table II. There are 8.79 valence electrons outside the APW sphere in the primitive cell. Each Ce APW sphere contains about 1.25 electrons in the f state. We have obtained similar results for the number of electrons in the f state per Ce APW sphere in CeSn<sub>3</sub>,<sup>17)</sup> CeNi,<sup>18)</sup> and CeRu<sub>2</sub>,<sup>19)</sup>, although there is difference in the number of electrons in the d state. We have also found that 0.1-0.2 electrons are contained in the f state of La APW sphere in corresponding La compounds and these elec-

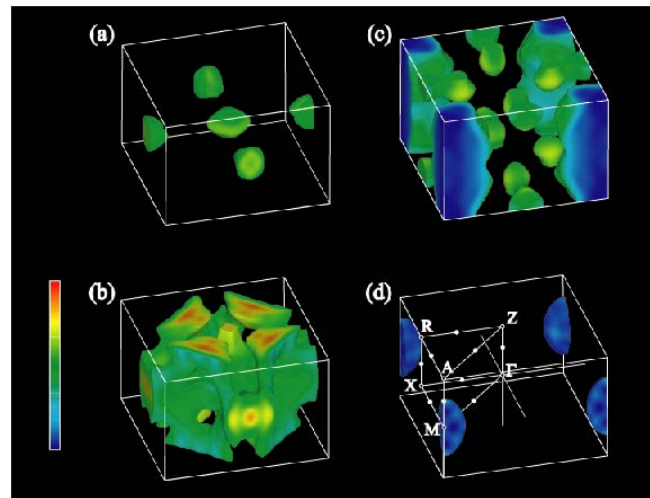


Fig. 3. Calculated Fermi surfaces of CeIrIn<sub>5</sub> for (a) 13th band hole sheets, (b) 14th band hole sheets, (c) 15th band electron sheets, and (d) 16th band electron sheets. Colors indicate the amount of 4f angular momentum character on each sheet of the Fermi surface. Red-shift indicate the increase of the admixture of f electrons. The center of the Brillouin zone is set at the point.

trons do not have an atomic character but a plane-wave character. This means that just one 4f electron per Ce atom becomes itinerant in the ground state in CeIrIn<sub>5</sub> and other paramagnetic Ce compounds.

The total density of states at  $E_F$  is evaluated as  $N(E_F) = 134.6$  states/Ryd.cell. By using this value, the theoretical specific heat coefficient  $\gamma_{\text{band}}$  is estimated as 23.3 mJ/K<sup>2</sup>mol. We note that the experimental electronic specific heat coefficient  $\gamma_{\text{exp}}$  is 750.0 mJ/K<sup>2</sup>mol. We define the enhancement factor for the electronic specific heat coefficient as  $\gamma = \gamma_{\text{exp}}/\gamma_{\text{band}} = 31.2$ . The disagreement between  $\gamma_{\text{band}}$  and  $\gamma_{\text{exp}}$  values is ascribed to electron correlation effect and electron-phonon interactions, which are not fully taken into account in the present LDA band theory.

Now let us discuss the Fermi surfaces of CeIrIn<sub>5</sub>. In Fig. 2, the lowest twelve bands are fully occupied. The next four bands are partially occupied, while higher bands are empty. Namely, the 13th, 14th, 15th, and 16th bands crossing the Fermi level construct the hole or electron sheet of the Fermi surface, as shown in Fig. 3. Note that the Fermi surfaces from 13th, 14th, 15th, and 16th bands are shown in (a), (b), (c), and (d). The Fermi surface from the 13th band consists of two equivalent small hole sheets centered at the X points and one hole sheet centered at the  $\Gamma$  point. The 14th band constructs a large hole sheet centered at the  $\Gamma$  point, which exhibits a complex network consisting of big "arms" which lie along the edges of Brillouin zone, as observed in Fig. 3 (b). The 15th band has two kinds of sheets, as shown in Fig. 3 (c). One is a set of two equivalent electron-like pockets, each of which is centered at the R point. A another sheet in the 15th band is a large cylindrical electron sheet which is centered at the M point. These electron sheets are characterized by two-dimensional Fermi surfaces. Namely,

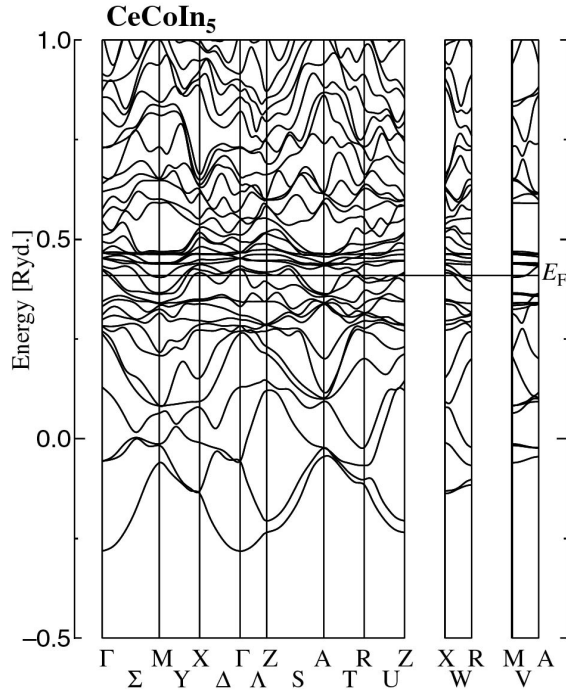


Fig. 4. Energy band structure calculated for CeCoIn<sub>5</sub> with the self-consistent R LAPW method.

they consist of the cylindrical sheet centered at the M point. The 16th band constructs a small electron sheet, which is centered at the M point, as shown in Fig. 3 (d). These Fermi surfaces are consistent with the previous results obtained by the full-potential linearized APW method,<sup>14)</sup> but here we point out a possible improvement on our relativistic band-structure calculation in the appearance of the Fermi surface shown in Fig. 3 (d), which has not been obtained in the previous band-structure calculations. The existence of the dHvA branch corresponding to this small Fermi surface does not contradict the present experimental results, but such a branch has not been yet identified. The number of carriers contained in these Fermi surface sheets are 0.039 holes/cell, 0.624 holes/cell, 0.626 electrons/cell and 0.037 electrons/cell in the 13th, 14th, 15th and 16th bands, respectively. The total number of holes is equal to that of electrons, which represents that CeIrIn<sub>5</sub> is a compensated metal.

Let us turn our attention to the analysis of the angular momentum character of the states forming various sheets of the Fermi surface. Here the most important quantity is the amount of Ce 4f character, which is the partial density of states for Ce 4f state for each point in k-space on the Fermi surface. This quantity is visualized in Fig. 3, where the admixture of the Ce 4f states is increased as the red shift in color, as shown in the scale diagram. The broad variation of the color from blue to red reflects a substantial variation of the 4f contribution for different groups of states which change in the range from about 5% to about 85%. However, this distribution is different from part to part on the Fermi surface.

Table III. The number of the valence electrons in the Ce APW sphere, the Co APW sphere, and the In APW sphere partitioned into angular momentum.

	s	p	d	f
Ce	0.29	6.16	2.11	1.28
Co	0.50	0.51	7.57	0.02
In (1c)	0.99	0.60	9.82	0.01
In (4i)	3.70	2.70	39.23	0.07

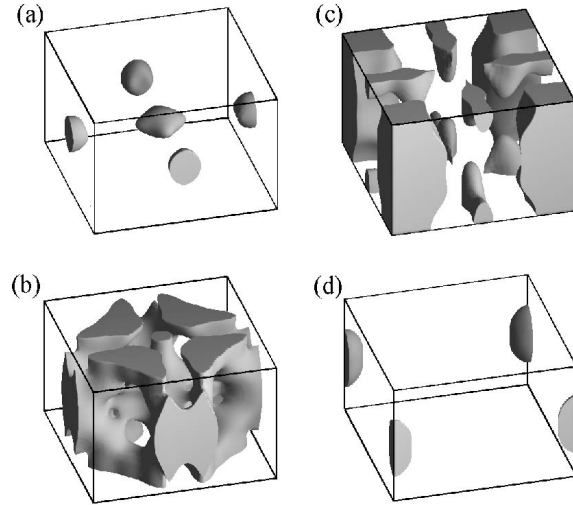


Fig. 5. Calculated Fermi surfaces of CeCoIn<sub>5</sub> for (a) 13th band hole sheets, (b) 14th band hole sheets, (c) 15th band electron sheets, and (d) 16th band electron sheets.

### 2.3 Results for CeCoIn<sub>5</sub>

In this subsection we will discuss the electronic properties of CeCoIn<sub>5</sub>. In Fig. 4, the energy band structure calculated for CeCoIn<sub>5</sub> is shown. Some remarks to depict this figure are the same as those in Fig. 2. First of all, we should note that there is no qualitative difference in the energy-band structure between CeIrIn<sub>5</sub> and CeCoIn<sub>5</sub>. Note, however, that the position of  $E_F$  is a little bit shifted as  $E_F = 0.409$  Ryd.

The occupation of the bands is also the same as that in CeIrIn<sub>5</sub>. Namely, the first twelve bands are fully occupied. The next four bands are partially occupied, while higher bands are empty. The number of the valence electrons in the APW sphere is listed for each angular momentum in Table III. There are 8.63 valence electrons outside the APW sphere in the primitive cell and each Ce APW sphere contains about 1.28 electrons in the f state. The total density of states is calculated at  $E_F$  as  $N(E_F) = 154.9$  states/Ryd.cell, leading to  $\chi_{\text{band}} = 26.8$  mJ/K<sup>2</sup> mol. Note that  $\chi_{\text{exp}} = 300.0$  mJ/K<sup>2</sup> mol for CeCoIn<sub>5</sub>, smaller than that of CeIrIn<sub>5</sub>, leading to  $\chi = 10.2$  small compared to that of CeIrIn<sub>5</sub>.

As for the Fermi surface, the situation is quite similar to CeIrIn<sub>5</sub>. Namely, the 13th, 14th, 15th and 16th bands construct the Fermi surface, as shown in Fig. 5. When

we compare them with those in Fig. 3, it is remarked that the shapes of the Fermi surfaces are essentially the same as those of CeIrIn<sub>5</sub>, although it is possible to point out difference of Fermi-surface structure in the orbits running around the bulges of the arms, which has center at the X point in the 14th band, and the topology of dumbbell, which has centered at the R point in the 15th band. Note also that these Fermi surfaces reproduce well the previous results.<sup>15)</sup> The numbers of carriers contained in these Fermi-surface sheets are 0.032 holes/cell, 0.627 holes/cell, 0.629 electrons/cell, and 0.030 electrons/cell in the 13th, 14th, 15th, and 16th bands, respectively. The total number of holes is equal to that of electrons, indicating that CeCoIn<sub>5</sub> is a compensated metal.

The small difference between those two compounds regarding the band structure around the Fermi level seems to be strange, if we recall the experimental facts such as T<sub>c</sub> and electronic specific heat coefficient  $c_{exp}$ . For CeIrIn<sub>5</sub>, T<sub>c</sub>=0.2K and  $c_{exp}=750.0 \text{ mJ/K}^2 \text{ mol}$ , while for CeCoIn<sub>5</sub> T<sub>c</sub>=2.3K and  $c_{exp}=300.0 \text{ mJ/K}^2 \text{ mol}$ . Namely, even though the band structure is similar to each other, the physical properties are quite different. This point is difficult to understand only within the present band-structure calculation results.

### 3. Tight-Binding Analysis

In the previous section we have focussed on the RLAPW band calculation results, in which the overall framework of the band structure around the Fermi energy E<sub>F</sub> is determined by the broad p band and the narrow f bands. We could obtain the Fermi surfaces consistent with the experimental results for both materials, although we have found an unexpected small difference in the energy bands between CeIrIn<sub>5</sub> and CeCoIn<sub>5</sub>.

In order to shed light on the problem, we consider the simplified effective model for CeTIn<sub>5</sub> by using the tight-binding method. For the purpose the two-dimensional lattice composed of Ce and In ions, are shown in Fig. 6, since the Fermi surfaces exhibit two-dimensionality, as has explained in the previous section. When we consider the tight-binding model on the two-dimensional lattice, it is enough to take 4f orbitals of Ce and 5p orbitals of In ions. In this sense, the model which we will construct is called the f-p model.

#### 3.1 f-p model

As easily deduced from Fig. 6, the f-p model Hamiltonian H should be written as

$$H = H_f + H_p + H_{fp} + H_{CEF}; \quad (3.1)$$

where the first and second term indicate the hopping of f and p electrons, respectively, while the third term denotes the f-p hybridization. The fourth term includes the effect of CEF. In the following we will consider each term. Note that in each term of H, we simply consider the nearest-neighbor hoppings of f- and p-electrons through bond, since our purpose here is a construction of a minimal tight-binding model to discuss magnetism and superconductivity by further adding Coulomb interactions.

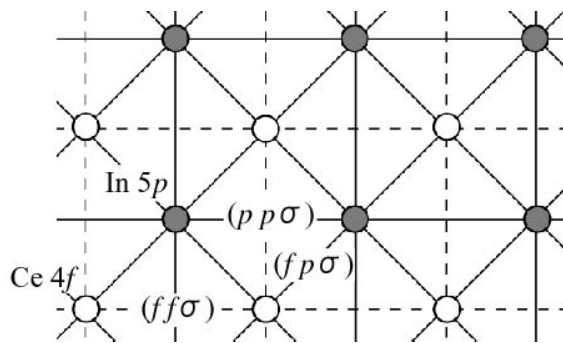


Fig. 6. Two-dimensional lattice composed of Ce and In ions. Open and hatched circles indicate the position of Ce and In ions, respectively.

First let us discuss the direct hopping process of f-electrons. Due to the spin-orbit coupling, the energy levels in Ce<sup>3+</sup> ion are split into j=5/2 sextet and j=7/2 octet. Since the magnitude of this splitting is as large as 0.4 eV, it is enough to consider only the j=5/2 sextet to evaluate the effective hopping of f electrons. The sextet in j=5/2 are labelled by m<sub>j</sub>=5/2, 3/2, 1/2, -1/2, -3/2, -5/2, with the z-component of j, but due to the time reversal symmetry, those states are classified into three pairs characterized by up and down "pseudo" spins.

When we define the second-quantized operator a<sub>i</sub> for the m<sub>j</sub>-state at site i, it is convenient to introduce the new operators f<sub>i</sub> with pseudospin as follows:

$$f_{ia} = a_{i5/2}; f_{i\#} = a_{i5/2}; \quad (3.2)$$

for "a" orbitals,

$$f_{ib} = a_{i1/2}; f_{i\#} = a_{i1/2}; \quad (3.3)$$

for "b" orbitals, and

$$f_{ic} = a_{i3/2}; f_{i\#} = a_{i3/2}; \quad (3.4)$$

for "c" orbitals. For the standard time reversal operator K = iγK, where K denotes the operator to take complex conjugate, we can easily show the relation

$$K f_i = f_i : \quad (3.5)$$

Note that this is the same definition for real spin.

Now we express the hopping term for f electrons as

$$H_f = \sum_{ia} t_{f0}^a \cdot f_{i0}^y f_{i+a0}^x; \quad (3.6)$$

where  $t_{f0}^a$  is the hopping amplitude of f electron between m<sub>j</sub>=0 and m<sub>j</sub>=0-orbitals in Ce<sup>3+</sup> ions connected by the vector a with a=x=(1, 0) and a=y=(0, 1). The hopping amplitude can be expressed as

$$t_{f0}^x = \frac{3}{56} (ff) \left( \begin{array}{ccc} 0 & p \frac{1}{10} & p \frac{1}{5} \\ p \frac{5}{10} & 2 & p \frac{1}{2} \\ p \frac{5}{5} & p \frac{1}{2} & 1 \end{array} \right) A; \quad (3.7)$$

and

$$t_{f0}^y = \frac{3}{56} (ff) \left( \begin{array}{ccc} 0 & p \frac{1}{10} & p \frac{1}{5} \\ p \frac{5}{10} & p \frac{1}{2} & p \frac{1}{2} \\ p \frac{5}{5} & 1 & 1 \end{array} \right) A; \quad (3.8)$$

where  $(ff)$  is the Slater-Koster integral between  $f$  orbitals through bond.<sup>20)</sup> Details for the derivation of hopping amplitude will be discussed elsewhere.<sup>21)</sup>

Next let us consider the  $p$ -electron hopping. In this case, it is not necessary to consider the effect of spin-orbit interaction at In site. Thus, we can consider the hopping of  $p$ -electrons with real spin and orbitals. Furthermore,  $p_z$  orbital does not contribute to the hopping process in the  $x$ - $y$  plane. Thus, it is enough to consider the hopping among  $m = \pm 1$  orbitals ( $m$  denotes the  $z$ -component of angular momentum), since  $p_z$  orbital is expressed only by the  $m = 0$  state among spherical harmonics for  $l = 1$ .

Note here that it is necessary to redefine spin and orbital also for  $p$  electrons, which should be consistent with those for  $f$  electrons, since we need to consider the  $f$ - $p$  mixing later. When we define the second-quantized operator  $c_{im}$  for the  $m$ -state with real spin, we can introduce new operators  $p_i$  as follows:

$$p_{ia} = c_{i1}; p_{i\#} = c_{i1\#}; \quad (3.9)$$

for "a" orbitals and

$$p_{ib} = c_{i1}; p_{i\#} = c_{i1\#}; \quad (3.10)$$

for "b" orbitals. Again we can easily show the relation

$$K p_i = p_i; \quad (3.11)$$

Note that this definition of pseudo spin is consistent with that of  $f$  electron.

After some algebraic calculations, we can obtain the  $p$ -electron hopping term as

$$H_p = \sum_{ia} t_p^a \sum_i p_i^y p_{ia}^y; \quad (3.12)$$

Where  $t_p^a$  is the hopping amplitude of  $p$ -electron between  $a$ - and  $0$ -orbitals in In ions connected by the vector  $a$ , given as

$$t_p^x = \frac{(pp)}{2} \begin{pmatrix} 1 & 1 \\ 1 & 1 \end{pmatrix}; \quad (3.13)$$

and

$$t_p^y = \frac{(pp)}{2} \begin{pmatrix} 1 & 1 \\ 1 & 1 \end{pmatrix}; \quad (3.14)$$

where  $(pp)$  is the Slater-Koster integral between  $p$  orbitals.

Note here that  $p$  electron hopping is expressed by the basis of spherical harmonics, not the cubic harmonics. Of course, only for the purpose to show the  $p$ -electron hopping, cubic harmonics can provide simpler expression, since non-zero hopping appears only between  $p_x$  ( $p_y$ ) orbitals along  $x$ - ( $y$ -) directions. However, when we include the  $f$ - $p$  hybridization, it is convenient to express it by using the basis of spherical harmonics.

Now we consider the  $f$ - $p$  hybridization term. In the present definitions of pseudo spins for  $f$ - and  $p$ -electrons, it is not necessary to distinguish the real and pseudo spins in the  $f$ - $p$  mixing term, if we pay due attention to the Clebsch-Gordan coefficients. Due to the similar calculations to derive  $f$ - $f$  and  $p$ - $p$  hopping term, we can

obtain the hybridization term as

$$H_{fp} = \sum_{ib} V_{ib}^b \sum_i f_i^y p_{ib}^y + h.c.; \quad (3.15)$$

where the hybridization is given by

$$V_{ib}^b = V_0 \begin{pmatrix} 0 & p \frac{1}{\sqrt{6}} & p \frac{1}{\sqrt{3}} \\ \frac{(fp)}{4} \frac{1}{\sqrt{7}} & p \frac{1}{\sqrt{6}} & p \frac{1}{\sqrt{3}} \end{pmatrix} A; \quad (3.16)$$

for  $b = [1=2; 1=2]$ . Note that  $b$  is the vector connecting neighbouring Ce and In ions. For  $b = [1=2; 1=2]$ ,  $V_{ib}^b = V_0$ . For down spins, we easily obtain

$$V_{ib}^b = V_{ib}^b; \quad (3.17)$$

By using the operators defined above, we can express the CEF term as

$$H_{CEF} = \sum_{i0} B_0 \sum_i f_i^y f_{i0}^y + \sum_i X \sum_i p_i^y p_i^y; \quad (3.18)$$

where  $B_0$  indicates the coefficients to express the effect of CEF and  $\epsilon$  is the energy level for  $p$ -orbitals measured from the  $f$  electron level. By consulting with the paper of Hutchings,<sup>22)</sup> it is easy to obtain for  $j = 5/2$  and tetragonal lattice as

$$\begin{aligned} B_{aa} &= 10B_2^0 + 60B_4^0; \\ B_{bb} &= 8B_2^0 + 120B_4^0; \\ B_{cc} &= 2B_2^0 + 180B_4^0; \\ B_{ac} &= B_{ca} = 12B_4^0; \end{aligned} \quad (3.19)$$

where  $B_p^q$  are the so-called CEF parameters.

All items included in the Hamiltonian have been established, but it is more convenient to express  $H$  in the momentum representation for the purpose to obtain the energy dispersion. After straightforward calculations of Fourier transformation, we finally obtain

$$\begin{aligned} H &= \sum_{k0} [(\epsilon_k^f + B_0) f_k^y f_k^y \\ &+ (\epsilon_k^p + \epsilon_0) p_k^y p_k^y \\ &+ (V_k^b \sum_i f_i^y p_{ik}^y + h.c.); \end{aligned} \quad (3.20)$$

where  $\delta_{ij}$  is the Kronecker delta and the  $f$ -electron energy is given by

$$\epsilon_k^f = \frac{3(ff)}{28} \begin{pmatrix} 0 & p \frac{1}{\sqrt{10}} & p \frac{1}{\sqrt{2}} \\ p \frac{1}{\sqrt{10}} & p \frac{1}{\sqrt{2}} & p \frac{1}{\sqrt{2}} \\ p \frac{1}{\sqrt{10}} & p \frac{1}{\sqrt{2}} & p \frac{1}{\sqrt{2}} \end{pmatrix} A; \quad (3.21)$$

with  $\epsilon_k = \cos k_x + \cos k_y$  and  $\epsilon_k = \cos k_x - \cos k_y$ . The  $p$ -electron energy is given as

$$\epsilon_k^p = (pp) \begin{pmatrix} \epsilon_k & \epsilon_k \\ \epsilon_k & \epsilon_k \end{pmatrix}; \quad (3.22)$$

and the hybridization is written by

$$V_{k0}^b = \frac{(fp)}{7} \begin{pmatrix} 0 & p \frac{1}{\sqrt{6}} & p \frac{1}{\sqrt{3}} \\ \frac{(fp)}{7} \frac{1}{\sqrt{7}} & p \frac{1}{\sqrt{6}} & p \frac{1}{\sqrt{3}} \end{pmatrix} A; \quad (3.23)$$

with  $c_k = \cos(k_x=2) \cos(k_y=2)$  and  $s_k = \sin(k_x=2) \sin(k_y=2)$ . Note that  $V_{k0}^b = V_{k0}^b$ .

### 3.2 Comparison with band calculation results

In the previous subsection, the  $f$ - $p$  model has been constructed by using seven parameters ( $ff$ ), ( $pp$ ), ( $fp$ ),  $B_2^0$ ,  $B_4^0$ , and  $B_4^4$ , which will be determined in the following conditions:

- (1) CEF parameters ( $B_2^0$ ,  $B_4^0$ ,  $B_4^4$ ) are determined from the experimental result for magnetic susceptibility.
- (2) The positions of the top and bottom of tight-binding bands correspond to point of the 25th and M point of 12th bands, respectively, in the RLAPW energy band structure. Note that those are mainly originating from the In 5p state.
- (3) The energy difference between  $f$  and  $p$  levels is determined to be positive due to the RLAPW band calculation results.
- (4) The  $f$  electron number per site is fixed as unity, since  $Ce^{3+}$  ion contains one  $f$  electron. However, the total number of electrons is not integer. It is difficult to reproduce quantitatively the band-structure calculation results (see, for instance, Table II) for electron numbers by a two-dimensional situation.
- (5) We should reproduce the Fermi surfaces constructed by the 13th, 14th and 15th bands, since they include significant  $f$ -electron contribution.
- (6) Inequalities  $(ff) < (pp)$  and  $(ff) < (fp)$  should hold, since  $p$  band is much wider than  $f$  band and  $f$ - $p$  mixing is large from the RLAPW results. Note, however, that the relation between  $(pp)$  and  $(fp)$  should be determined by the parameter fitting.

First let us analyze the energy bands and Fermi surfaces of  $CeIrIn_5$  based on the  $f$ - $p$  model. As for CEF parameters, we can determine them as  $B_2^0 = 15K$ ,  $B_4^0 = 0.52K$ , and  $B_4^4 = 0.47K$  from the experimental results for magnetic susceptibility.<sup>23)</sup> In Fig. 7 (a), we plot  $(fp)$  and  $(pp)$  as a function of  $\Delta$  for  $(ff) = 4400K$ , as a typical example to explain the fitting procedure. Note that we determine the parameters in the two-dimensional tight-binding model by comparing with the three-dimensional band-structure calculation results. Thus, the present  $(ff)$  inevitably becomes large compared with the actual value in the three-dimensional system. We can see three regions regarding the number of Fermi surfaces: One for  $\Delta < 1800$  (region-I), two for  $1800 < \Delta < 2100$  (region-II), and three for  $2100 < \Delta < 2500$  (region-III and IV). Due to the condition (5), we need three Fermi surfaces. Note, however, that for  $\Delta > 2500$  (region-IV),  $(fp)$  becomes smaller than  $(ff)$ , although we obtain three Fermi surfaces, which is in contradiction to condition (6). Thus, we discard the region-IV and choose only region-III, namely,  $2100 < \Delta < 2500$ .

Note that  $f$ -electron number is fixed to unity from the condition (4) as shown in Fig. 7 (b), while  $p$  electron number  $n_p$  is not fixed. However, as shown in Fig. 8 (b),  $n_p$  is almost 1.5, irrespective of  $\Delta$ . If we consult with the band-structure calculation results, as shown in Table I,  $n_p = 0.66$ , since we consider the two-dimensional plane consisting of  $Ce$  and  $In(1c)$  ions. Although the band-structure calculation has been done in the three-dimensional situation, the  $f$ - $p$  model is constructed by assuming pure two-dimensions. Thus, the discrepancy in  $n_p$  between the band-structure calculation and tight-binding

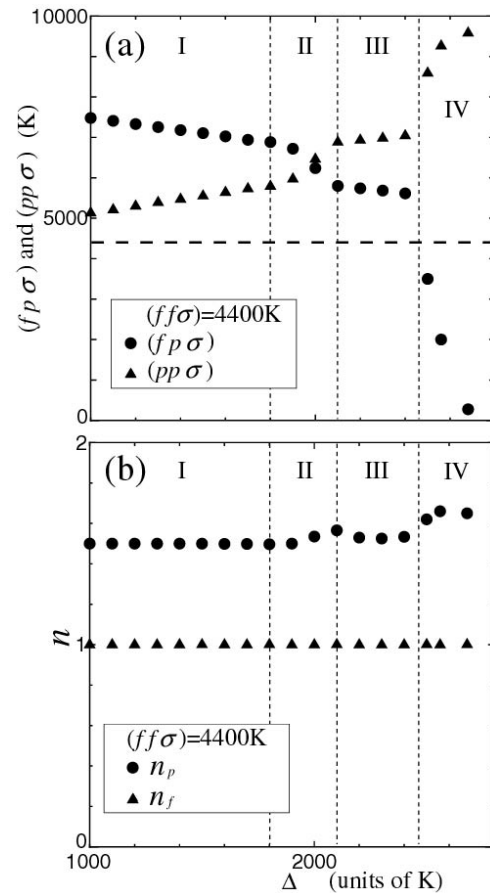


Fig. 7. (a)  $(fp)$  and  $(pp)$  as a function of  $\Delta$  for  $(ff) = 4400K$ . Note that the horizontal hashed line indicate the energy of  $(ff)$ . (b)  $f$  and  $p$  electron number per site as a function of  $\Delta$ .

model is not primary problem in the following. It may be possible to consider that the present  $f$ - $p$  model is contacted with the "reservoir" of  $p$  electrons, namely, In (4i) sites, indicating that  $n_p$  should not be determined only within the simple two-dimensional tight-binding model.

After depicting the same figures as Fig. 7 (a) for several values of  $(ff)$ , we can determine some region in parameter space to satisfy the conditions (1)–(6). In Fig. 8 (a), we show a typical result for  $(ff) = 4400K$  and  $\Delta = 2300K$  with  $(pp) = 6980K$  and  $(fp) = 5685K$ . The Fermi level is located at the bottom of the  $Ce$  4f bands. The states near  $E_F$  have strong  $Ce$  4f character, although they include some In 5p admixture. There are three bands crossing  $E_F$  along the  $-M$  lines. Among them two cross also  $E_F$  along the  $X-M$  direction, leading to two large cylindrical sheets of Fermi surface. As shown by solid curves in Fig. 8 (b), the Fermi surface of the tight-binding model from the first band consists of one hole sheet centered at the  $\Gamma$  point. The second band constructs a cylindrical electron sheet centered at the  $M$  point, as shown by the solid curves in Fig. 8 (c). There exist tiny Fermi surfaces around  $X$ -point, although such Fermi surfaces in the RLAPW results shown by dotted curves in Fig. 8 (b), not in Fig. 8 (c). This disagreement may be due to the simplification of the  $f$ - $p$  model, but such tiny Fermi surfaces are not important in the following analysis. The third band constructs a small cylindrical electron sheet



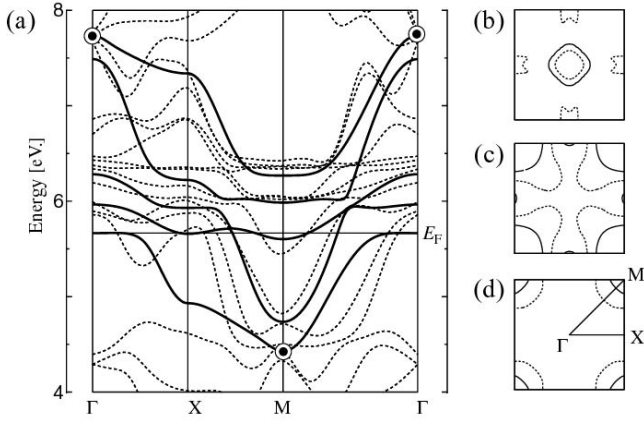


Fig. 8. (a) Energy band structures around  $E_F$  for CeIrIn<sub>5</sub>. The solid and dashed curves indicate the results for tight-binding and the RLAPW calculation, respectively. Adjusted RLAPW energy levels are denoted by the circled dots. Fermi-surface lines discussed here are (b) 13th band hole sheets, (c) 14th band hole sheets, and (d) 15th band electron sheets. In (b)–(d), solid and dotted curves denote the Fermi-surface lines for the tight-binding model and the RLAPW results, respectively.

centered at the M point, as shown in Fig. 8(d). In total, the overall feature of energy bands around the Fermi level are well reproduced by the simplified f-p model.

Now we turn our attention to CeCoIn<sub>5</sub>. CEF parameters of this compound have been determined experimentally as  $B_2^0 = 6.8K$ ,  $B_4^0 = 0.05K$ , and  $B_4^4 = 2.5K$ .<sup>24)</sup> By using these CEF parameters, we have attempted to reproduce the band-structure calculations, and finally we can obtain Fig. 9 for  $T = 2300K$ ,  $(pp) = 5730K$ ,  $(fp) = 5360K$ , and  $(ff) = 4400K$ . Again we see that major features of the energy bands of CeCoIn<sub>5</sub> are basically similar to those of CeIrIn<sub>5</sub>. The behavior of the hybridization of energy bands and the relative position of the 4f-bands to the other valence bands are not changed when we compare with those of CeIrIn<sub>5</sub>. In fact, the obtained Fermi surfaces are essentially the same as those of CeIrIn<sub>5</sub>, as easily understood from the comparison between Figs. 8 and 9.

Here let us consider the meaning of similarity between those two compounds. In the f-p model we have seven parameters, which are classified into two groups, i.e., high- and low-energy groups. The high-energy group includes  $(ff)$ ,  $(pp)$ ,  $(fp)$ , and  $\lambda$ , while low-energy group consists of CEF parameters,  $B_2^0$ ,  $B_4^0$ , and  $B_4^4$ . Note here that the typical energy scale is 1000K for the former, while at most 10K for the latter group. The energy band structure with the RLAPW method around the Fermi energy  $E_F$  is mainly determined by high-energy group parameters. On the other hand, the band structure is not sensitive to CEF parameters, since those are much smaller than the typical energy scale considered in the band-structure calculations. In fact, the resolution of the energy band structure with the RLAPW method is less than the energy scale of CEF parameters. Thus, the smallness of difference between CeIrIn<sub>5</sub> and CeCoIn<sub>5</sub> suggests that CEF parameters are important to characterize the difference in Ce-115 materials. This is con-

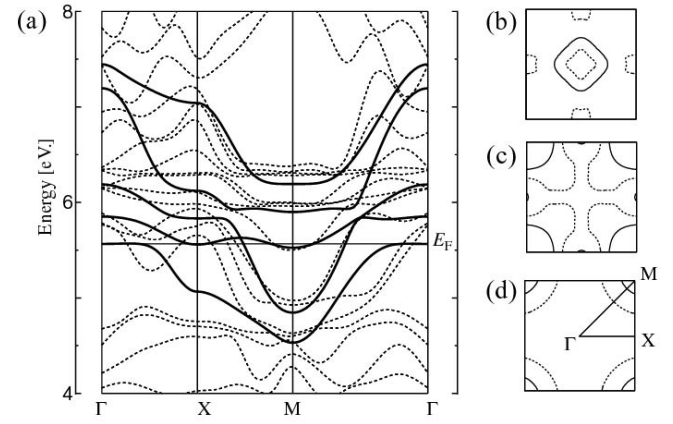


Fig. 9. (a) Energy band structures around  $E_F$  for CeCoIn<sub>5</sub>. Meanings of all notations are the same as those in Fig. 8. Fermi-surface lines shown here are (b) 13th band hole sheets, (c) 14th band hole sheets, and (d) 15th band electron sheets.

sistent with another experimental analysis for magnetic excitations.<sup>25)</sup>

### 3.3 Role of CEF parameters in Ce-115 compounds

Since we have confirmed that the overall band-structure is well reproduced by the tight-binding f-p model, let us now discuss the role played by the CEF parameters in Ce-115 materials based on the f-p model from the qualitative viewpoint. Note again that the effect of CEF parameters cannot be discussed in the RLAPW results, since it is included only partially in the band-structure calculations. In order to see the effect of CEF parameters on the band-structure, we consider two types of modification in CEF parameters for CeIrIn<sub>5</sub>: In Fig. 10(a),  $B_2^0$  is just increased as  $10B_2^0$  by keeping others invariant, while only  $B_4^0$  is increased as  $10B_4^0$  in Fig. 10(b). As for  $B_4^4$ , we show no figure, since the band-structure is not changed significantly, even if we change it as  $100B_4^4$ . Namely,  $B_4^4$  is the most insensitive quantity among three CEF parameters, and thus, we do not discuss the effect of  $B_4^4$  furthermore.

In Figs. 10(a) and (b), it is noted that there is clear difference in the tendency of the change in the band-structure when we increase  $B_2^0$  or  $B_4^0$ . Here note that the solid curves indicate the results for increasing CEF parameter. When we increase  $B_2^0$ , the energy bands are totally shifted upward, as observed in Fig. 10(a). On the other hand, for the increase of  $B_4^0$ , the distance between two bands forming the Fermi surfaces tend to be narrow, as shown in Fig. 10(b). Here we focus on two bands forming the main Fermi surfaces, second and third solid curves in Fig. 8 from the bottom, since those Fermi surfaces with large volume in the Brillouin zone includes significant amount of f electrons. Note that this narrowing effect due to the increase of  $B_4^0$  occurs only in bands around the Fermi level, although the shift due to the change of  $B_2^0$  seems to occur in all bands.

It is considered that the physical quantities are sensitive to  $B_4^0$ , since those are determined by the band-structure around the Fermi level. For instance, due

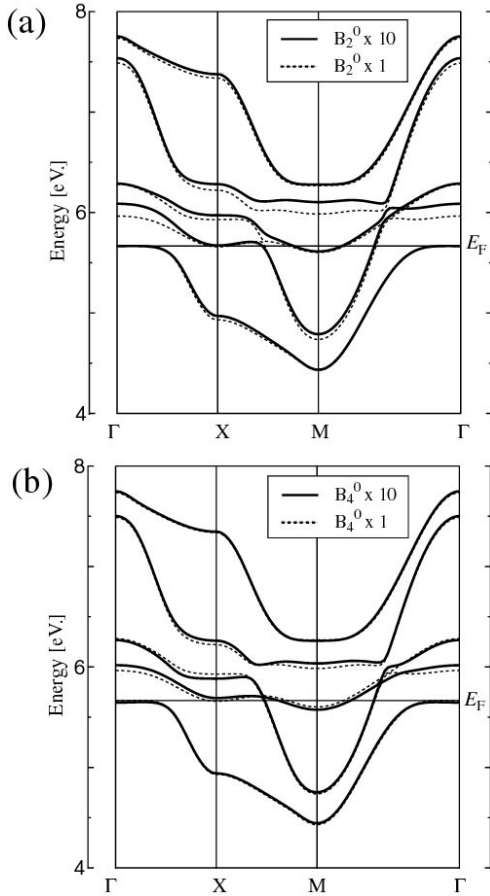


Fig. 10. Energy band structures of the  $f$ - $p$  model around  $E_F$  for  $\text{CeIrIn}_5$  when we increase (a) only  $B_2^0$  and (b) only  $B_4^0$ , by keeping other parameters invariant. The Fermi level for the band structure for  $10B_2^0$  is fixed as that for  $B_2^0$ , and  $f$ -electron number is unity from the condition (4).

to the narrowing effect of effective band-width around the Fermi level,  $N(E_F)$  (the density of states at the Fermi level) should be increased with increasing  $B_4^0$ . Here we recall the experimental results on CEF parameters such as  $B_4^0 = 0.52\text{K}$  for  $\text{CeIrIn}_5$  and  $B_4^0 = 0.05\text{K}$  for  $\text{CeCoIn}_5$ . Due to the present discussion, we can conclude that  $N(E_F)$  of  $\text{CeIrIn}_5$  becomes larger than that of  $\text{CeCoIn}_5$ , if we correctly include the effect of CEF in the band-structure calculations. In fact, we have observed that  $\chi_{\text{exp}} = 750.0 \text{ mJ/K}^2 \text{ mol}$  and  $300.0 \text{ mJ/K}^2 \text{ mol}$  for  $\text{CeIrIn}_5$  and  $\text{CeCoIn}_5$ , respectively. We emphasize that the difference in  $\chi_{\text{exp}}$  can be understood, at least qualitatively, by taking into account the effect of CEF parameters into the  $f$ - $p$  model. It is a clear advantage to consider the electronic properties based on the present tight-binding model, since the effect of CEF parameters can be included in an explicit manner.

Here it should be also noted that at present, electron correlations have not been included explicitly. In general, in actual heavy-fermion materials, quantities with small energy scale such as CEF parameters can be significant, since the energy scale of quasi-particles is much reduced due to the large renormalization effect. In this sense, it may be considered that our present analysis on the CEF parameters has been done effectively on the tight-

binding model for quasi-particles, since we compare it with the band-structure calculation results, even though correlation effects have not been satisfactorily included in the band-structure calculations. In any case, in order to obtain definite conclusion on this issue, further quantitative works to include electron correlations are needed in future.

Finally, let us try to consider a possible scenario to understand the difference in  $T_c$  between  $\text{CeCoIn}_5$  and  $\text{CeIrIn}_5$ . It may be risky to conclude something regarding superconductivity without considering seriously the effect of electron correlations, since superconductivity in  $\text{Ce-115}$  materials has been believed to be originating from antiferromagnetic spin fluctuations.<sup>26)</sup> However, it is an interesting trial to discuss the effect of  $B_4^0$  on  $T_c$  to clarify the importance of CEF parameters in  $\text{Ce-115}$  materials. As discussed above, the increase in  $B_4^0$  induces the effective narrowing of the band-width around the Fermi level. Thus, it is deduced that electron correlation becomes effectively larger as  $B_4^0$  is increased. In fact, for  $\text{CeRhIn}_5$  which is an antiferromagnet at ambient pressure,  $B_4^0$  is estimated as  $0.55\text{K}$ ,<sup>23)</sup> which is slightly larger than that of  $\text{CeIrIn}_5$ . This is consistent with the present conclusion. By following our discussion, it may be possible to conclude that the magnitude of antiferromagnetic spin fluctuations should be larger in the order of  $\text{CeCoIn}_5$ ,  $\text{CeIrIn}_5$ , and  $\text{CeRhIn}_5$ , in agreement with the previous discussion on the effect of level splitting to control antiferromagnetic spin fluctuations.<sup>26)</sup> Of course, the present discussion on superconductivity is just in a qualitative level, but we believe that the effect of CEF should be one of key issues to distinguish the difference in  $\text{Ce-115}$  materials, in combination with the large renormalization effect due to electron correlations.

#### 4. Summary

In this paper, we have applied the RLAPW method to the self-consistent calculation of the electronic structure for  $\text{CeIrIn}_5$  and  $\text{CeCoIn}_5$  on the basis of the itinerant  $4f$  electron picture. We have found that a hybridization between the  $\text{Ce } 4f$  state and  $\text{In } 5p$  state occurs in the vicinity of  $E_F$ . The obtained main Fermi surfaces are composed of two hole sheets and one electron sheet, all of which are constructed from the band having the  $\text{Ce } 4f$  state and the  $\text{In } 5p$  state.

In order to understand the difference in electronic properties between  $\text{CeIrIn}_5$  and  $\text{CeCoIn}_5$  even though the energy-band structure around the Fermi level are quite similar to each other, we have constructed the  $f$ - $p$  model based on the knowledge of the RLAPW band calculation. It has been found that the size and position of the main Fermi surfaces for the  $f$ - $p$  model agree with the RLAPW ones. By further analyzing the  $f$ - $p$  model, we have concluded that  $B_4^0$  among the CEF parameters plays an important role to determine electronic properties, consistent with the experimental results observed in  $\text{CeIrIn}_5$  and  $\text{CeCoIn}_5$ .

Here it is emphasized that the system can be sensitive to such small energy quantities as CEF parameters, since the energy scale of the electron system is much reduced due to the large renormalization effect in heavy-fermion

compound. Namely, our present conclusion is based on the pre-formation of heavy quasi-particles. To complete the discussion, we need to treat both the effect of CEF and electron correlation at the same footing on the basis of the microscopic model, for instance, the f-p model with Coulomb interactions. This point will be discussed elsewhere in future.

In order to make further step to quantitative discussion on superconductivity, it is also necessary to analyze the model, in which short-range Coulomb interaction terms are added to the present tight-binding model or more simplified f-electron model,<sup>27)</sup> leading to a microscopic Hamiltonian to discuss magnetism and superconductivity of f-electron systems.<sup>26)</sup> We believe that in this paper we show one route to arrive at the elucidation of the mechanism of unconventional superconductivity in heavy fermion materials.

#### Acknowledgements

We thank M. Higuchi, Y. Onuki, P. G. Pagliuso, and T. Takimoto for discussions. T. H. and K. U. are supported by the Grant-in-Aid for Scientific Research from Japan Society for the Promotion of Science.

- [1] P. Hohenberg and W. Kohn: Phys. Rev. 136 (1964) 864; W. Kohn and L. J. Sham: Phys. Rev. 140 (1965) A1133.
- [2] For recent developments in the band-structure calculation techniques, see, for instance, V. V. Nemoshkalenko and V. N. Antonov: Computational Methods in Solid State Physics, (Golden and Beach Science Publishers, New York, 1998).
- [3] M. J. P. Perdew: in Electronic structure of solids '91, edited by P. Ziesche and H. Eschrig (Akademie, Berlin, 1991) pp. 11; A. D. Becke: J. Chem. Phys. 96 (1992) 2155.
- [4] V. I. Anisimov, J. Zaanen, and O. K. Andersen: Phys. Rev. B 44 (1991) 943; V. I. Anisimov, I. V. Solovyev, M. A. Korotin, M. T. Czyzyk, and G. A. Sawatzky: Phys. Rev. B 48 (1993) 16929.
- [5] Y. Maeno, T. M. Rice, and M. Sigrist: Physics Today 54 (2001) 42 and references are therein.
- [6] See, for instance, T. Takimoto: Phys. Rev. B 62 (2000) R14641.
- [7] T. L. Loucks, Augmented Plane Wave Method (Benjamin, New York, 1967).
- [8] A. Hasegawa and H. Yamagami: Prog. Theo. Phys. Suppl. 108 (1992) 27.
- [9] H. Yamagami and A. Hasegawa: J. Phys. Soc. Jpn. 59 (1990) 2426.
- [10] M. Higuchi and A. Hasegawa: J. Phys. Soc. Jpn. 64 (1995) 830.
- [11] H. Hegger, C. Petrovic, E. G. Moshopoulou, M. F. Hundley, J. L. Sarrao, Z. Fisk, and J. D. Thompson: Phys. Rev. Lett. 84 (2000) 4986.
- [12] C. Petrovic, R. Movshovich, M. Jaime, P. G. Pagliuso, M. F. Hundley, J. L. Sarrao, Z. Fisk, and J. D. Thompson: Europhys. Lett. 53 (2001) 354.
- [13] C. Petrovic, P. G. Pagliuso, M. F. Hundley, R. Movshovich, J. L. Sarrao, J. D. Thompson, Z. Fisk, and P. Monthoux: J. Phys.: Condens. Matter 13 (2001) L337.
- [14] Y. Haga, Y. Inada, H. Harima, K. Okawa, M. Murakawa, H. Nakawaki, Y. Tokiwa, D. Aoki, H. Shishido, S. Ikeda, N. Watanabe, and Y. Onuki: Phys. Rev. B 63 (2001) 060503(R).
- [15] R. Settai, H. Shishido, S. Ikeda, Y. Murakawa, M. Nakashima, D. Aoki, Y. Haga, H. Harima, and Y. Onuki: J. Phys.: Condens. Matter 13 (2001) L627.
- [16] O. K. Andersen: Phys. Rev. B 12 (1975) 3060.
- [17] A. Hasegawa, H. Yamagami, and H. Johbetoh: J. Phys. Soc. Jpn. 59 (1990) 2457.
- [18] H. Yamagami and A. Hasegawa: J. Phys. Soc. Jpn. 60 (1991) 1011.
- [19] M. Higuchi and A. Hasegawa: J. Phys. Soc. Jpn. 65 (1996) 1302.
- [20] J. C. Slater and G. F. Koster: Phys. Rev. 94 (1954) 1498.
- [21] T. Hotta and K. Ueda: preprint.
- [22] M. T. Hutchings: Solid State Phys. 16 (1965) 227.
- [23] T. Takeuchi, T. Inoue, K. Sugiyama, D. Aoki, Y. Tokiwa, Y. Haga, K. Kondo, and Y. Onuki: J. Phys. Soc. Jpn. 70 (2001) 877.
- [24] H. Shishido, R. Settai, D. Aoki, S. Ikeda, H. Nakawaki, N. Nakamura, T. Iizuka, Y. Inada, K. Sugiyama, T. Takeuchi, K. Kondo, T. C. Kobayashi, Y. Haga, H. Harima, Y. Aoki, T. Namiki, H. Sato, and Y. Onuki: J. Phys. Soc. Jpn. 71 (2001) 162.
- [25] P. G. Pagliuso, N. J. Curro, N. O. Moreno, M. F. Hundley, J. D. Thompson, J. L. Sarrao, and Z. Fisk: to be published in Physica B (2002).
- [26] T. Takimoto, T. Hotta, T. M. Aehira, and K. Ueda: J. Phys.: Condens. Matter, 14 (2002) L369.
- [27] T. M. Aehira, T. Takimoto, T. Hotta, K. Ueda, M. Higuchi, and A. Hasegawa: J. Phys. Soc. Jpn. 71 (2002) Suppl. A, 285.